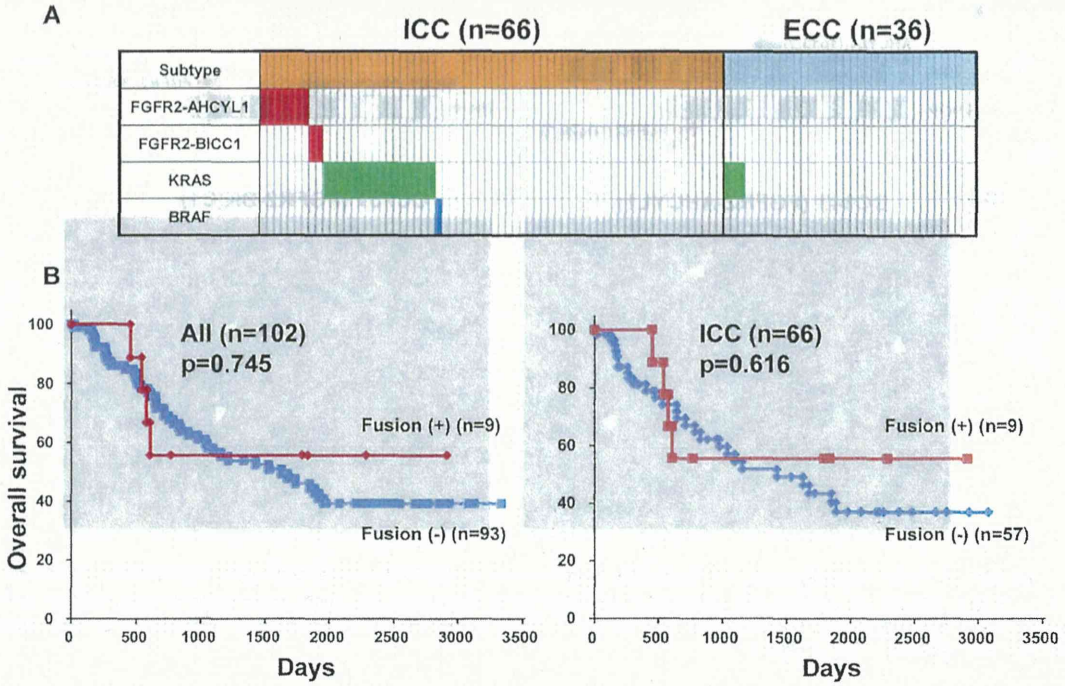

Fig. 3. Clinical subtypes in cholangiocarcinoma. (A) Distribution of genomic alterations. *FGFR2* fusion, *KRAS* mutation, and *BRAF* mutation among ICC and ECC cases are indicated by red, green, and blue, respectively. (B) Overall survival curve stratified by *FGFR2* fusions in all cholangiocarcinoma cases and ICC cases (Kaplan-Meier method). The outcome was not significantly different between *FGFR2* fusion-positive and -negative cases (log-rank test).

canonical FGFR signaling and confer anchorage-independent growth and *in vivo* tumorigenesis, both of which are hallmarks of cellular transformation.

FGFR2 Fusions Are Potential Therapeutic Targets in Cholangiocarcinoma. Next, we examined the sensitivity of *FGFR2* fusion-driven tumor cells to two specific FGFR inhibitors, BGJ398 and PD173074, which selectively inhibit FGFR tyrosine kinase activity.[18,19] These compounds significantly inhibited the phosphorylation of MAPK and reduced *in vitro* anchorage-independent colony formation to the level observed in KD mutant expressing cells (Fig. 5B).

Discussion

FGFR genes are involved in multiple biological processes, ranging from cell transformation, angiogenesis, and tissue repair, to embryonic development. Activating point mutations and amplification of *FGFR* gene members have been explored as therapeutic targets in a wide range of tumors, including bladder, gastric, and lung cancers[20,21]; however, amplification of *FGFR* genes is uncommon in ICC.[22] Diverse fusions involving the *FGFR* gene family have also been reported in hematological and solid cancers[10,11,23,24] and some have shown sensitivity to FGFR inhibition.

The identification of two recurrent *FGFR2* fusions (*FGFR2-AHCYL1* and *FGFR2-BICC1*) that are mutually exclusive with *KRAS/BRAF* mutations warrants a new molecular classification of cholangiocarcinoma and suggests a novel therapeutic approach in cholangiocarcinomas driven by these fusions. Wu et al.[11] recently detected the *FGFR2-BICC1* fusion gene in two cholangiocarcinoma cases, although its prevalence

Table 2. Association Between Clinical Features and FGFR2 Fusion

Clinical factors		Number of fusion positive case	Number of fusion negative case	*P* Value
Gender	Male	4	61	0.207
	Female	5	32	
Age (average)		62.1	66.1	0.104
Virus status	Hepatitis virus positive	3	9	0.035
	Hepatitis virus negative	6	84	
Differentiation	Well	4	21	0.367
	Mod	5	60	
	Poor	0	5	
Stage	I	1	2	0.463
	II	2	14	
	III	2	30	
	IV	4	23	

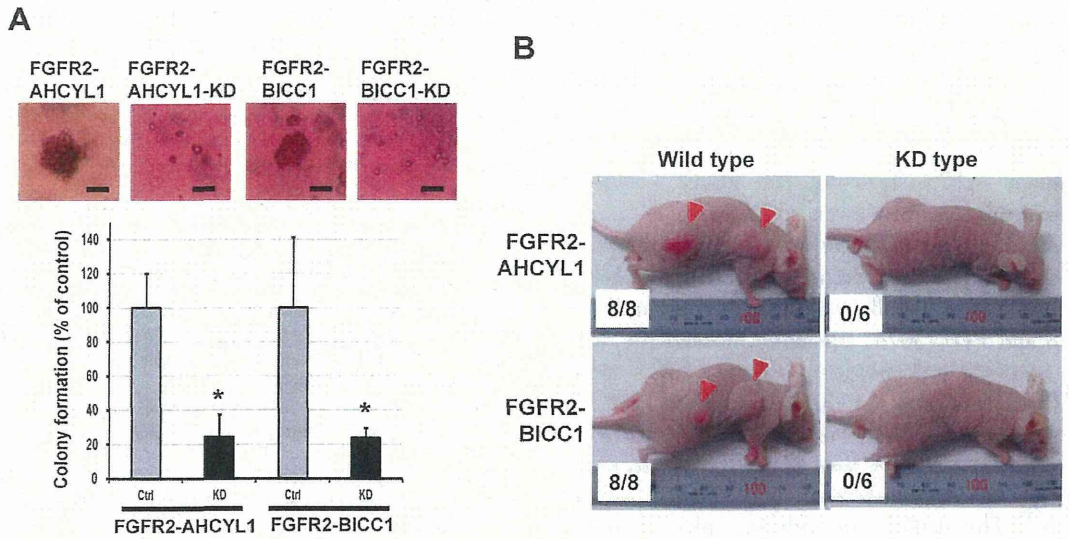

Fig. 4. Oncogenic activity of FGFR2 fusion proteins. (A) Soft agar colony formation in kinase activity-deficient (KD) mutants. The percentage (±SD) of colonies with FGFR2 fusions and their KD mutant transfectants are plotted. $*P < 0.05$. A representative image of colonies expressing wild-type and KD FGFR2 fusions is shown (scale bar = 100 μm). (B) Representative images of mice subcutaneously transplanted with NIH3T3 cells expressing wild-type and KD FGFR2 fusions. The number of tumors per injection in each transfectant is shown.

in cholangiocarcinoma has been lacking. The present study showed a high prevalence of *FGFR2* fusion genes in the intrahepatic subtype of cholangiocarcinoma. Although two cases of another kinase fusion, *FIG-ROS1* (2/23, 8.7%), have been reported by other researchers in CC,[10] we did not detect such fusion in this study. As cholangiocarcinoma is a heterogeneous disease, some epidemiological or clinical specificity may be ascribable to the *FIG-ROS1* fusion. However, no detailed pathological information of the patients was stated in that study. Further investigation is needed to clarify the whole picture of driver fusion genes in CC. Association between *FGFR2* fusion positivity and hepatitis virus infection may suggest an involvement of the virus in the chromosomal rearrangements in CC. However, rare observation of *FGFR2* fusion in hepatocellular carcinoma argues for further analysis of genetic rearrangements.

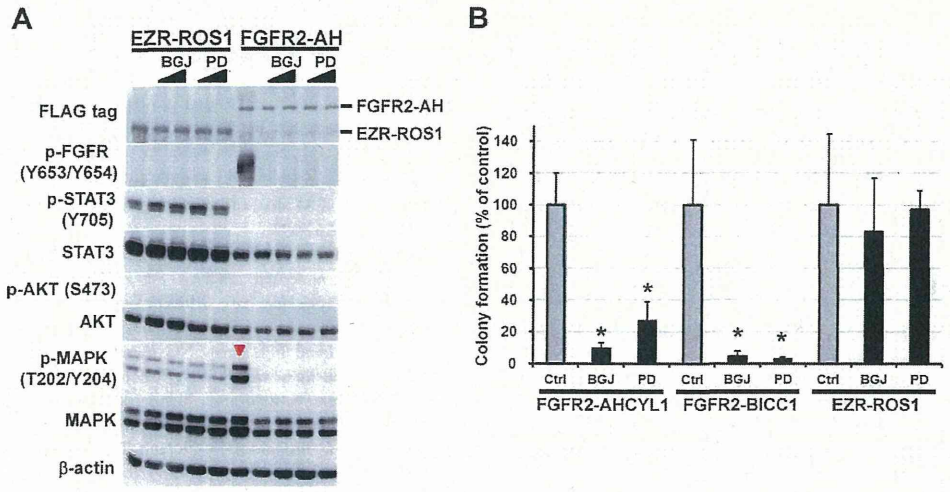

Fig. 5. FGFR inhibitors block signaling in FGFR2-fusion-expressing cells. (A) Activation of FGFR2 and MAPK by FGFR2-AHCYL1 and its suppression by FGFR inhibitors. Lysates from NIH3T3 cells expressing FGFR2-AHCYL1 or EZR-ROS1 (control) treated with vehicle (DMSO), 0.2 and 1 μM BGJ398, and 0.2 and 1 μM PD173074 were immunoblotted with the relevant antibodies. β-Actin was used as a loading control. (B) Anchorage-independent growth of NIH3T3 cells expressing FGFR2 fusions and its suppression by FGFR inhibitors (BGJ: BGJ398 and PD: PD173074). The percentage (±SD) of colonies formed in the presence of FGFR2 inhibitors (0.2 μM) with respect to those formed by DMSO-treated cells are plotted. The NIH3T3 clone expressing EZR-ROS1 was used as a negative control for FGFR inhibitors. $*P < 0.05$.

Overexpression of the FGFR2 fusion protein hyperactivate one of the canonical signaling events downstream of FGFR. This contrast with other FGFR fusion proteins, FGFR1-TACC1 and FGFR3-TACC3 in glioblastoma,[24] which fail to activate canonical downstream MAPK signaling, but induce aneuploidy and oncogenic transformation.[9]

Based on the specific relevant genomic alterations, TKIs have been developed into effective therapies.[7,8] We showed that small molecule FGFR inhibitors, BGJ398 and PD173074, efficiently blocked the downstream signaling and oncogenic activity of ICC-specific *FGFR2* fusions. By the high-throughput cell line profiling assay, amplifications or mutations of *FGFR* genes in cancer cell lines have been reported to predict sensitivity to the selective pan-FGFR inhibitor BGJ398.[25] This drug is currently in a phase I study in patients of advanced solid tumors with FGFR1/2 amplification or FGFR3 mutation (Novartis, Basel, Switzerland; ClinicalTrials.gov identifier: NCT01004224). Clinical investigations, akin to those conducted in other solid tumors with oncogenic fusion kinases, such as *EML4-ALK*,[26] are warranted to examine the efficacy of FGFR inhibitors for the treatment of defined subset of cholangiocarcinoma harboring *FGFR2* fusions.

Acknowledgment: We thank S. Wakai, H. Shimizu, S. Ohashi, W. Mukai, T. Urushidate, and N. Okada of the National Cancer Center for excellent technical assistance.

Author Contributions: Sequencing and data analysis: Y.T., N.H., H.N., F.H.; Molecular biological analysis: Y.A., F.H.; Clinical and pathological analysis: T.Shirota., H.O., K.F., K.S., T.O., T.K.; Article writing: Y.A., Y.T., F.H., T.S.; Study design: Y.A., Y.T., T. Shibata.

References

1. Razumilava N, Gores GJ. Classification, diagnosis, and management of cholangiocarcinoma. Clin Gastroenterol Hepatol 2013;11:13-21.
2. Khan SA, Thomas HC, Davidson BR, Taylor-Robinson SD. Cholangiocarcinoma. Lancet 2005;366:1303-1314.
3. Ong, CK, Subimerb C, Pairojkul C, Wongkham S, Cutcutache I, et al. Exome sequencing of liver fluke-associated cholangiocarcinoma. Nat Genet 2012;44:690-693.
4. Voss JS, Holtegaard LM, Kerr SE, Barr Fritcher EG, Roberts LR, Gores GJ, et al. Molecular profiling of cholangiocarcinoma shows potential for targeted therapy treatment decisions. Hum Pathol 2013; 44:1216-1222.
5. Hezel AF, Zhu AX. Systemic therapy for biliary tract cancers. Oncologist 2008;13:415-423.
6. Aljiffry M, Abdulelah A, Walsh M, Peltekian K, Alwayn I, Molinari M. Evidence-based approach to cholangiocarcinoma: a systematic review of the current literature. J Am Coll Surg 2009;208:134-147.
7. Mitelman F, Johansson B, Mertens F. The impact of translocations and gene fusions on cancer causation. Nat Rev Cancer 2007;7:233-245.
8. Ablain J, Nasr R, Bazarbachi A, de The H. The drug-induced degradation of oncoproteins: An unexpected Achilles' heel of cancer cells? Cancer Discov 2011;1:117-127.
9. Gerber DE, Minna JD. ALK inhibition for non-small cell lung cancer: from discovery to therapy in record time. Cancer Cell 2010;18:548-551.
10. Gu TL, Deng X, Huang F, Tucker M, Crosby K, Rimkunas V, et al. Survey of tyrosine kinase signaling reveals ROS kinase fusions in human cholangiocarcinoma. PLoS One 2011;6:e15640.
11. Wu YM, Su F, Kalyana-Sundaram S, Khazanov N, Ateeq B, Cao X, et al. Identification of targetable FGFR gene fusions in diverse cancers. Cancer Discov 2013; 3:636-647.
12. Kohno T, Ichikawa H, Totoki Y, Yasuda K, Hiramoto M, Nammo T, et al. KIF5B-RET fusions in lung adenocarcinoma. Nat Med 2012;18: 375-377.
13. Arai Y, Totoki Y, Takahashi H, Nakamura H, Hama N, Kohno T, et al. Mouse model for ROS1-rearranged lung cancer. PLoS One 2013; 8:e56010.
14. Ando H, Mizutani A, Matsu-ura T, Mikoshiba K. IRBIT, a novel inositol 1,4,5-trisphosphate (IP3) receptor-binding protein, is released from the IP3 receptor upon IP3 binding to the receptor. J Biol Chem 2003; 278:10602-10612.
15. Wessely O, Tran U, Zakin L, De Robertis EM. Identification and expression of the mammalian homologue of Bicaudal-C. Mech Dev 2001;101:267-270.
16. Kim CA, Bowie JU. SAM domains: uniform structure, diversity of function. Trends Biochem Sci 2003;28:625-628.
17. Brooks AN, Kilgour E, Smith PD. Molecular pathways: fibroblast growth factor signaling: a new therapeutic opportunity in cancer. Clin Cancer Res 2012;18:1855-1862.
18. Skaper SD, Kee WJ, Facci L, Macdonald G, Doherty P, Walsh FS. The FGFR1 inhibitor PD 173074 selectively and potently antagonizes FGF-2 neurotrophic and neurotropic effects. J Neurochem 2000;75:1520-1527.
19. Guagnano V, Furet P, Spanka C, Bordas V, Le Douget M, Stamm C, et al. Discovery of 3-(2,6-dichloro-3,5-dimethoxy-phenyl)−1-{6-[4-(4-ethyl-piperazin-1-yl)-phenylamino]-pyrimidin-4-yl}-1-methyl-urea (NVP-BGJ398), a potent and selective inhibitor of the fibroblast growth factor receptor family of receptor tyrosine kinase. J Med Chem 2011;54:7066-7083.
20. Turner N, Grose R. Fibroblast growth factor signaling: from development to cancer. Nat Rev Cancer 2010;10:116-129.
21. Weiss J, Sos ML, Seidel D, Peifer M, Zander T, Heuckmann JM, et al. Frequent and focal FGFR1 amplification associates with therapeutically tractable FGFR1 dependency in squamous cell lung cancer. Sci Transl Med 2010;2:62ra93.
22. Sia D, Hoshida Y, Villanueva A, Roayaie S, Ferrer J, Tabak B, et al. Integrative molecular analysis of intrahepatic cholangiocarcinoma reveals 2 classes that have different outcomes. Gastroenterology 2013; 144:829-840.
23. Chase A, Grand FH, Cross NC. Activity of TKI258 against primary cells and cell lines with FGFR1 fusion genes associated with the 8p11 myeloproliferative syndrome. Blood 2007;110:3729-3734.
24. Singh D, Chan JM, Zoppoli P, Niola F, Sullivan R, Castano A, et al. Transforming fusions of FGFR and TACC genes in human glioblastoma. Science 2012;337:1231-1235.
25. Guagnano V, Kauffmann A, Wöhrle S, Stamm C, Ito M, Barys L, et al. FGFR genetic alterations predict for sensitivity to NVP-BGJ398, a selective pan-FGFR inhibitor. Cancer Discov 2012;2:1118-1133.
26. Kwak EL, Bang YJ, Camidge DR, Shaw AT, Solomon B, Maki RG, et al. Anaplastic lymphoma kinase inhibition in non-small-cell lung cancer. N Engl J Med 2010;363:1693-1703.

Acta Neuropathol
DOI 10.1007/s00401-015-1403-6

ORIGINAL PAPER

Evolution of DNA repair defects during malignant progression of low-grade gliomas after temozolomide treatment

Hinke F. van Thuijl · Tali Mazor · Brett E. Johnson · Shaun D. Fouse · Koki Aihara · Chibo Hong · Annika Malmström · Martin Hallbeck · Jan J. Heimans · Jenneke J. Kloezeman · Marie Stenmark-Askmalm · Martine L. M. Lamfers · Nobuhito Saito · Hiroyuki Aburatani · Akitake Mukasa · Mitchell S. Berger · Peter Söderkvist · Barry S. Taylor · Annette M. Molinaro · Pieter Wesseling · Jaap C. Reijneveld · Susan M. Chang · Bauke Ylstra · Joseph F. Costello

Received: 30 December 2014 / Revised: 21 February 2015 / Accepted: 21 February 2015

Abstract Temozolomide (TMZ) increases the overall survival of patients with glioblastoma (GBM), but its role in the clinical management of diffuse low-grade gliomas (LGG) is still being defined. DNA hypermethylation of the *O*^{6}*-methylguanine-DNA methyltransferase* (*MGMT*) promoter is associated with an improved response to TMZ treatment, while inactivation of the DNA mismatch repair (MMR) pathway is associated with therapeutic resistance and TMZ-induced mutagenesis. We previously demonstrated that TMZ treatment of LGG induces driver mutations in the RB and AKT–mTOR pathways, which may drive malignant progression to secondary GBM. To better understand the mechanisms underlying TMZ-induced mutagenesis and malignant progression, we explored the evolution of *MGMT* methylation and genetic alterations affecting MMR genes in a cohort of 34 treatment-naïve LGGs and their recurrences. Recurrences with TMZ-associated hypermutation had increased *MGMT* methylation compared to their untreated initial tumors and higher overall *MGMT* methylation compared to TMZ-treated non-hypermutated recurrences. A TMZ-associated mutation in one or more MMR genes was observed in five out of six TMZ-treated hypermutated recurrences. In two cases, pre-existing heterozygous deletions encompassing *MGMT*, or an MMR gene, were followed by TMZ-associated mutations in one of the genes of interest. These results suggest that tumor cells with methylated *MGMT* may

Electronic supplementary material The online version of this article (doi:10.1007/s00401-015-1403-6) contains supplementary material, which is available to authorized users.

H. F. van Thuijl · T. Mazor · B. E. Johnson · S. D. Fouse · C. Hong · M. S. Berger · A. M. Molinaro · S. M. Chang · J. F. Costello (✉)
Department of Neurological Surgery, University of California San Francisco, San Francisco, CA, USA
e-mail: joseph.costello@ucsf.edu

H. F. van Thuijl · J. J. Heimans · J. C. Reijneveld
Department of Neurology, VU University Medical Center, Amsterdam, The Netherlands

H. F. van Thuijl · P. Wesseling · B. Ylstra
Department of Pathology, VU University Medical Center, Amsterdam, The Netherlands

K. Aihara · N. Saito · A. Mukasa
Department of Neurosurgery, The University of Tokyo, Tokyo, Japan

K. Aihara · H. Aburatani
Genome Science Laboratory, Research Center for Advanced Science and Technology, The University of Tokyo, Tokyo, Japan

A. Malmström
Department of Advanced Home Care, Linköping University, Linköping, Sweden

A. Malmström · M. Hallbeck · M. Stenmark-Askmalm · P. Söderkvist
Department of Clinical and Experimental Medicine, Linköping University, Linköping, Sweden

J. J. Kloezeman · M. L. M. Lamfers
Department of Neurosurgery, Brain Tumor Center, Erasmus Medical Center, Rotterdam, The Netherlands

M. Stenmark-Askmalm
Department of Clinical Pathology and Clinical Genetics, University Hospital, Linköping, Sweden

B. S. Taylor
Department of Epidemiology and Biostatistics, Memorial Sloan Kettering Cancer Center, New York, NY, USA

Published online: 28 February 2015

undergo positive selection during TMZ treatment in the context of MMR deficiency.

Keywords Low-grade glioma · Temozolomide · Hypermutator · Mismatch repair · *MGMT*

Introduction

Diffuse LGG are infiltrative brain tumors which include World Health Organization (WHO) grade II astrocytomas, oligodendrogliomas, and oligoastrocytomas [32]. Surgical resection is the primary therapeutic intervention, though LGG recur and may undergo malignant progression to a higher histological grade including grade IV secondary GBM. Therefore, in patients with clinical risk factors [41, 50], postoperative adjuvant treatment is often utilized. The addition of TMZ to postoperative radiotherapy prolongs progression-free survival (PFS) and overall survival (OS) in high-risk LGG patients, and chemotherapy instead of irradiation might be as effective [3, 45] and defers the risk of late radiation-induced cognitive deterioration [14]. Moreover, postoperative TMZ or irradiation of LGG has been associated with improved quality of life, better seizure control, and longer progression-free survival [6, 29, 37, 42, 48].

Temozolomide is an alkylating agent that methylates the O^6 position of guanine. The DNA repair protein MGMT removes O^6-methyl groups induced by TMZ. Initial studies assaying DNA methylation in the *MGMT* gene body rather than promoter showed a direct correlation between *MGMT* methylation and expression [19, 40]. When the *MGMT* promoter is hypermethylated, however, *MGMT* expression is decreased and TMZ-induced DNA damage persists [12, 13]. O^6-methylguanine pairs with thymine instead of cytosine during DNA replication. MMR can recognize and repair these mismatches through MutS and MutL complexes. MSH2 and MSH6 form the MutSα complex, which identifies base–base mismatches and small insertion–deletion loops (IDLs). MSH2 and MSH3 form the MutSβ complex, which identifies large IDLs. MutS complexes directly with MutL, an MLH1/PMS2 dimer, to the site of DNA damage [20, 21]. Removal of the thymine that is base paired with O^6-methylguanine is followed by repair synthesis that reinserts thymine, leading to repeated attempts to repair the same base. This futile cycling of repair has been linked to DNA double-strand breaks and apoptosis, the apparent mechanism of TMZ-induced cytotoxicity [16].

Inactivation of the MMR pathway is a mechanism of resistance to TMZ in primary GBMs and also leads to TMZ-induced mutagenesis [8, 18, 26, 62]. In MMR-deficient cells, the base pairing of O^6-methylguanine with thymine persists, and upon DNA replication results in nucleotide transitions from guanine to adenine. TMZ-associated hypermutation has been observed in GBM [9–12], in cells treated with TMZ in vitro [8] and in unpaired post-treatment tissue samples [1, 5, 15, 16, 26]. In contrast to MMR, the impact of MGMT activity on the relative amount of cytotoxicity versus mutagenicity is much less clear. Furthermore, while *MGMT* methylation is associated with longer overall survival in GBM patients treated with TMZ [25], it is unclear whether this biomarker has the same prognostic value in patients with *IDH1* mutated LGG [17, 53, 58].

We recently identified hypermutation in a subset of TMZ-treated recurrent GBMs that arose from *IDH1*-mutant astrocytic LGG [28]. Post-TMZ recurrences had a 39- to 133-fold increase in the mutation rate relative to their treatment-naïve initial LGG, more than 98 % of which are C>T/G>A mutations which are associated with TMZ-induced mutagenesis (Supplementary Table S1) [5]. TMZ-associated mutations resulted in deregulation of RB-mediated cell cycle control and hyperactivated AKT–mTOR signaling, suggesting TMZ-induced hypermutation may drive malignant progression. However, it is unclear why hypermutation developed in only six of the ten LGG treated with TMZ. To better understand the mechanism of hypermutation, here we examined the stepwise development of DNA repair deficiency and subsequent TMZ-associated hypermutation using a cohort of 34 initial LGG and their patient-matched recurrence, including 23 pairs for which exome sequencing data were available. Because TMZ-induced hypermutation in LGG was associated exclusively with GBM recurrence, this study is important for understanding and ultimately avoiding TMZ-associated hypermutation and malignant progression.

Methods

Sample acquisition

Patient inclusion in this cohort was dependent upon (1) an initial diagnosis of WHO grade II diffuse astrocytoma, oligodendroglioma, or oligoastrocytoma; (2) available tumor

B. S. Taylor
Human Oncology and Pathogenesis Program, Memorial Sloan Kettering Cancer Center, New York, NY, USA

A. M. Molinaro
Department of Epidemiology and Biostatistics, University of California San Francisco, San Francisco, CA, USA

P. Wesseling
Department of Pathology, Radboud University Nijmegen, Nijmegen, The Netherlands

J. C. Reijneveld
Department of Neurology, Academic Medical Center, University of Amsterdam, Amsterdam, The Netherlands

tissue from an initial tumor and a subsequent recurrence; (3) information on post-surgical treatment. A majority of the samples have been used in previous studies (Supplementary Table S2) [28, 55]. Tumor samples were fresh frozen or formalin-fixed paraffin-embedded (FFPE) tissues. Sample use was approved by the Committee on Human Research at UCSF; the Ethics Committee of the University of Tokyo; and the Medical Ethics Committees of the Dutch hospitals VU University Medical Center Amsterdam, Radboud University Medical Center Nijmegen, Isala Klinieken Zwolle and Erasmus Medical Center Rotterdam, and the Linköping University Hospital, Sweden.

DNA isolation

Genomic DNA from tumor and normal tissue samples of patients 01-38 was either extracted with the QIAGEN FFPE DNA extraction kit (Qiagen, Valencia, CA, USA) following the manufacturer's instructions or isolated by a standard phenol chloroform extraction as previously described [28]. FFPE blocks of initial tumor and recurrences of patients 90–302 were cut into sections of 3–5 μm thickness for pathological evaluation on hematoxylin and eosin-stained slides. For each sample, an area was delineated that contained >60 % tumor cells. The corresponding area on subsequent sections of 10 μm was used for DNA isolation extracted with the QIAGEN FFPE DNA extraction kit [55].

Bisulfite treatment, PCR, cloning and sequencing of *MGMT*

O^6-methylguanine-DNA methyltransferase methylation status was assessed for all patients (Fig. 1a and Fig. S1) [24]. DNA (>100 ng) was bisulfite treated for 2.5 h with the EZ DNA methylation Gold kit (Zymo Research, Irvine, California) according to the manufacturer's instructions. Bisulfite-converted DNA was amplified by PCR using the following primers corresponding to the MGMT promoter: forward GGATATGTTGGGATAGTT and reverse ATCGTTAATAAGTCAAGCTC. Gel extraction of the amplified DNA was performed with the QIAEXII gel extraction Kit (Qiagen, Germantown, Maryland). Four to six microliters of PCR product was cloned using a pCR2.1/TOPO TA sequencing kit (Invitrogen, Carlsbad, CA, USA). Individual bacterial clones were subjected to PCR using vector-specific primers and a minimum of nine individual PCR clones were sequenced per tumor sample. Bisulfite sequence data of the *MGMT* promoter were analyzed with BISMA [47]. The bisulfite conversion rate was monitored in all reactions at non-CpG cytosines, which are typically unmethylated and converted. For comparison, the methylation status of the *MGMT* promoter in bisulfite-treated DNA was also determined in a subset of the samples by standard, non-quantitative methylation-specific PCR (MSP) [16].

Identification of somatic mutations and copy number aberrations in *MGMT* and MMR genes

The identification of MMR pathway alterations was limited to those for which sufficient tumor DNA and matched normal DNA was available for exome sequencing. The mutational and copy number status of *MGMT* as well as the key MMR pathway genes *MLH1*, *MLH3*, *MSH2*, *MSH3*, *MSH5*, *MSH6*, *PMS1*, and *PMS2* [27] were assessed from the exome sequencing data. For patients 01–24, somatic mutations and copy number aberrations in genes of interest were identified as previously described [28]. Nine new exome sequencing datasets were also generated for this study using the Agilent SureSelect Target Enrichment System Protocol (Version 1.0 September 2009) with the SureSelect Human All Exon 50 Mb kit (Agilent Technologies) according to the manufacturer's instructions. Paired-end reads of 76 or 100 bp in length were generated from Illumina HiSeq 2000 or 2500 instrumentation. Paired-end sequencing data from exome capture libraries were aligned to the reference human genome (build hg19) with the Burrows–Wheeler Aligner (BWA) 0.5.10 [31]. Single-nucleotide variants (SNVs) were detected with MuTect [11], and indels were detected with Pindel [61], followed by custom filters to remove false positives [28]. All candidate mutations were subsequently validated with PCR amplification of the target region from tumor and matched normal genomic DNA followed by conventional Sanger sequencing. Copy number segmentation was performed with an adaptation of circular binary segmentation (CBS) [28, 56]. We identified germline heterozygous SNPs from the matched normal exome of each patient tumor using the UnifiedGenotyper [34]. From only those SNPs present in dbSNP (Build ID: 132) (http://www.ncbi.nlm.nih.gov/SNP/) and with a coverage level of 10 or more reads, we calculated their minor allele frequency in all exomes of each patient (initial tumor, recurrence, and patient-matched normal) and used these to infer genomic regions with loss of heterozygosity (LOH). Regions of LOH were then correlated with DNA copy number alterations. For patients 171–296 copy number aberrations at genes of interest were identified from low-coverage whole-genome sequencing as previously described [49, 55]. Copy number segmentation was performed by CBS [28] and gains and losses were identified using CGHcall [54].

Significance tests

For differences in methylation, the initial comparison between subgroups was done using the Kruskal–Wallis test (the nonparametric alternative to ANOVA), followed by subsequent post hoc testing using the Wilcoxon rank-sum or signed-rank test (on data from tumor pairs) for two group analyses. *P* values below 0.05 were considered statistically significant.

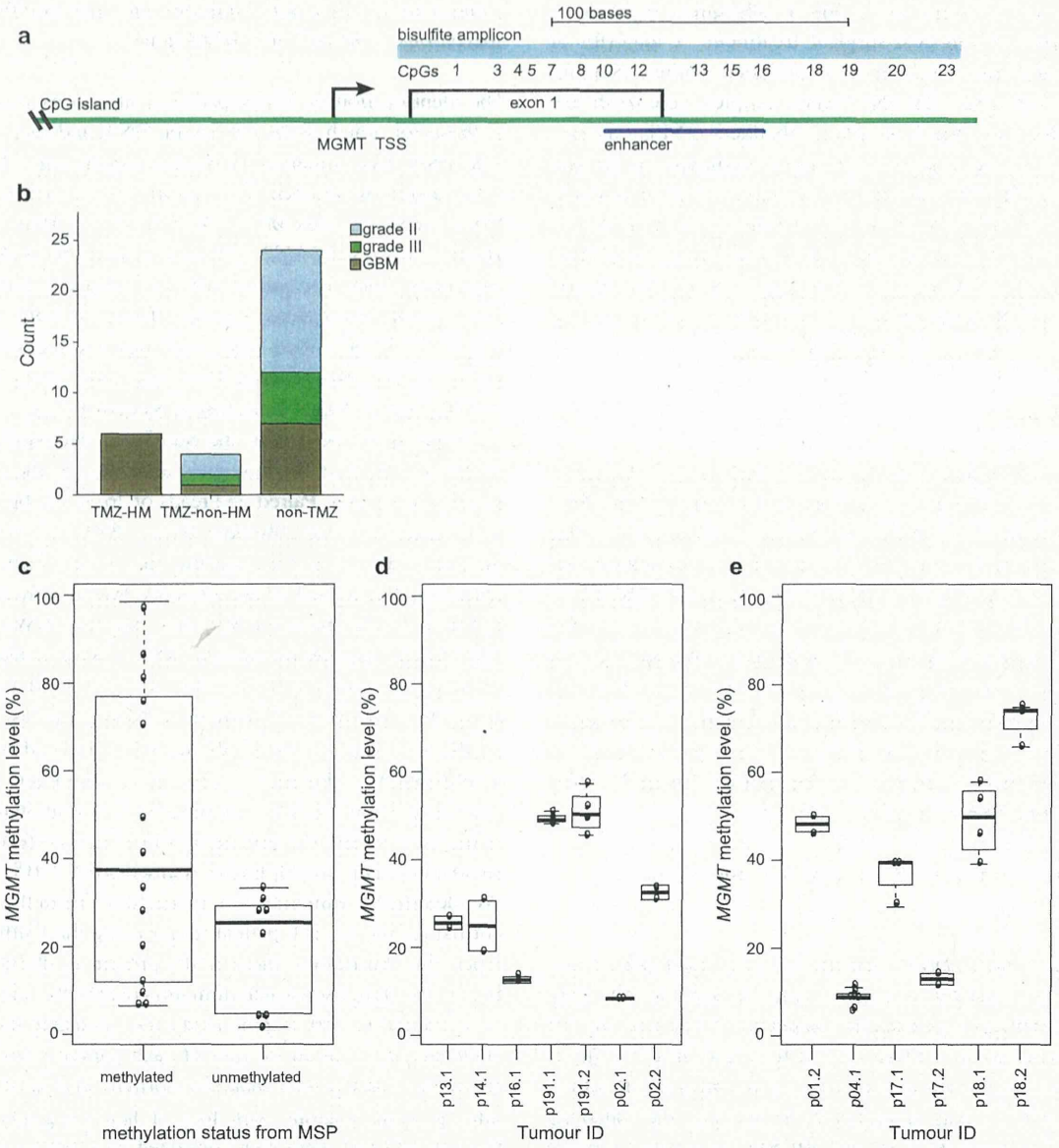

Fig. 1 Comparison of *MGMT* methylation in different assays and across tumor regions. **a** Position of the *MGMT* bisulfite amplicon (*light blue*) encompassing the 23 CpGs assessed in this study, the position of the *MGMT* CpG island (*green*), and the enhancer region encompassing CpGs 10–16 (*dark blue*). *TSS* transcription start site. **b** Distribution of histological subtypes and grades of the recurrent tumors in the three groups. **c** Comparison of the binary outcome of MSP (*x* axis) to *MGMT* methylation level of CpGs 10–16 determined by bisulfite, PCR and sequencing of 10 or more independent clones (*y* axis). **d** The degree of variation in methylation levels was determined in replicate experiments from independent aliquots of the same genomic DNA isolation (*y* axis) with bisulfite and sequencing of the *MGMT* promoter in individual samples (*x* axis). **e** *MGMT* methylation levels (*y* axis) in spatially distinct regions of individual tumors (*x* axis). Sample designations are the patient (p) number followed by 0.1 for initial tumor and 0.2 for the recurrent tumor

Results

Histological features and disease course of the cohort

Clinical and genomic data for many of the paired initial and recurrent tumor samples used in this study have been described previously [28, 55]. In total, we studied 87 samples from 34 LGG patients. Samples from spatially distinct regions of the tumor were available for six surgeries. Ten of the 34 patients received adjuvant TMZ. Accordingly, we divided the cohort into three groups based on the clinical and exome sequencing data; patients with recurrent tumors

displaying a TMZ-associated hypermutator phenotype (TMZ-HM, $n = 6$), TMZ-treated patients without a TMZ-associated hypermutator phenotype (TMZ-non-HM, $n = 4$) and patients not treated with TMZ (non-TMZ, $n = 24$) (Supplementary Table S2). While the overall size of the cohort is relatively modest, very few studies have reported genomic and epigenomic evolution in similarly sized cohorts of paired initial LGG and recurrent tumors [57]. In the TMZ-HM group, all six tumors recurred with GBM histology. Relative to the TMZ-HM group, the number of recurrent tumors with GBM histology was variable in the TMZ-non-HM group and non-TMZ group, (ANOVA, p value 0.013) (Fig. 1b).

MGMT methylation level is similar across assays, technical replicates and spatially distinct samples

Methyl-specific PCR (MSP) is used in clinical tests for *MGMT* methylation status and yields a low-resolution, non-quantitative binary call of methylated or unmethylated. However, *MGMT* methylation levels in tumors span a full range from unmethylated to fully methylated at each CpG. We therefore compared MSP to a more quantitative, single-CpG resolution method involving bisulfite treatment, PCR, cloning and sequencing in 18 samples. The genomic region assessed by the bisulfite sequencing approach assesses methylation level at each of 23 CpG sites in the *MGMT* promoter and enhancer including the region covered by the MSP assay which spans CpG sites 10–16 [2, 33], a previously reported differentially methylated region 2 (DMR2) covered by CpGs 3–20 [33], and CpG site 13 which has prognostic value in GBMs [2] (Fig. 1a). In eight samples, classified as *MGMT* unmethylated by MSP, median methylation level was 25.4 % (range 1.6–28.6 %), and in ten samples that were methylated according to MSP, median methylation level was 37.4 % (range 6.5–98.6 %) (Fig. 1c). To test the reproducibility of bisulfite sequencing approach, experiments of seven samples were repeated on independent aliquots from the same genomic DNA isolation. Very little variation in methylation level was observed between replicate experiments (Fig. 1d). An analysis of spatially distinct regions in samples obtained from the same surgery revealed that there was also very little variation in *MGMT* methylation levels within a tumor at a given time point (Fig. 1e). This limited intratumoral heterogeneity of *MGMT* methylation level provided evidence that the result of a single sample was likely to be representative for LGG, as previously shown in GBM [15, 21, 23].

Increase in MGMT methylation level associated with temozolomide-induced hypermutation

MGMT methylation levels varied widely between patients. Across the whole cohort, the median methylation level of initial tumors was 29.7 % (range 6.1–70.9 %) and the median methylation level of recurrent tumors was also 29.7 % (range 3.9–79.1 %), (p value 0.49) (Supplementary Material). Between the three subgroups, median methylation levels in initial tumors were not significantly different (TMZ-HM 38.3 % vs. TMZ-non-HM 17.8 %, p value 0.15; TMZ-HM vs. non-TMZ 33 %, p value 0.33), while overall methylation level in recurrent tumors of the TMZ-HM group (median 55 %) was significantly higher compared to recurrent tumors of the TMZ-non-HM (median 20 %) and non-TMZ (median 28 %) groups (p value 0.013 and 0.03, respectively) (Fig. 2). Patient 24 was not included in this analysis, as methylation data were confounded by low tumor purity in the initial and first recurrent tumor, complicating the interpretation.

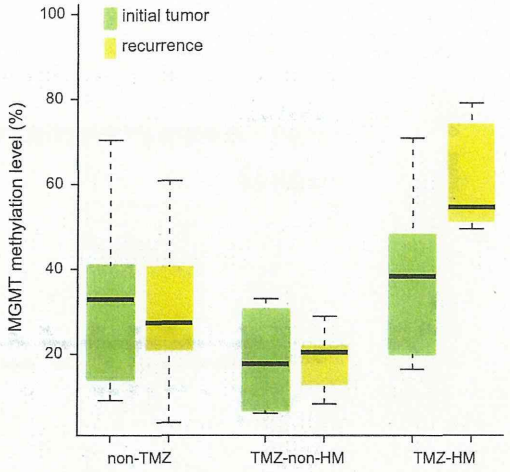

Fig. 2 Significantly elevated *MGMT* methylation in TMZ-associated hypermutated recurrent tumors that arise from LGG. *MGMT* methylation levels in initial (*green*) and recurrent (*yellow*) tumors of three patient subgroups. *non-TMZ* patients not treated with TMZ, *TMZ-non-HM* patients treated with TMZ without a hypermutated recurrent tumor, *TMZ-HM* patients treated with TMZ with a hypermutated recurrent tumor

We explored how methylation levels changed over time by performing paired analysis in initial and recurrent tumors of the three subgroups TMZ-HM, TMZ-non-HM, non-TMZ. The change in methylation level from initial to recurrence in the TMZ-HM group was non-significant but showed a trend (p value 0.063). This is supported by the consistent increase in methylation level in this subgroup. This pattern was significantly different from the variable patterns of change over time in the TMZ-non-HM and non-TMZ groups (TMZ-HM vs. TMZ-non-HM p value 0.050; TMZ-HM vs. non-TMZ p value 0.005) (Fig. 2). Eleven of 23 individual CpGs were significantly more methylated in the recurrent tumors of the subgroups TMZ-HM vs. TMZ-non-HM (CpGs 1–6, 8–10, 12 and 13, p values 0.012–0.044).

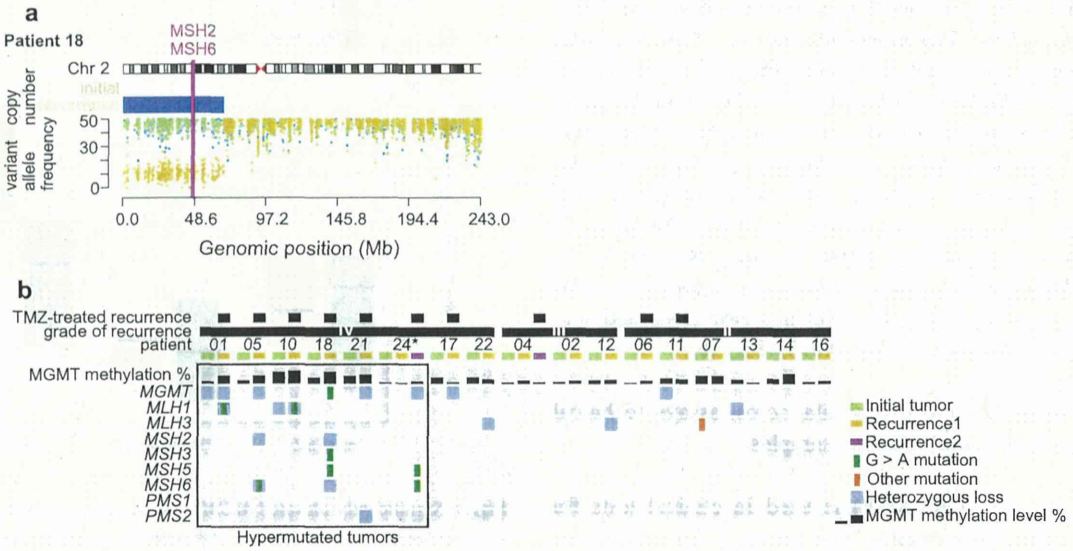

Fig. 3 Sequential acquisition of DNA repair deficiency exclusively in LGG patients treated with TMZ and had a hypermutated recurrence. **a** Exome-derived copy number status and germline variant allele frequency across chromosome 2 encompassing *MSH2* and *MSH6* in the initial and recurrent tumor of patient 18. **b** Methylation level of *MGMT*, mutations and copy number status of *MGMT* and MMR-related genes in initial LGG and paired recurrent tumors. The panel includes patients for whom exome sequencing data were available, *Asterisk* indicates samples with a proportion of tumor cells lower than 50 %

Evolution of DNA repair deficiency in the TMZ-HM group

In the initial tumors of the TMZ-HM group ($n = 6$), no MMR gene mutations were detected, however, DNA repair may have been impaired by the heterozygous loss of *MGMT* in patient 01 and *MLH1* in patient 10. In contrast, five of the six TMZ-HM GBMs contained a TMZ-associated mutation in one of the MMR genes, concurrent with deletion of the other allele or deletion encompassing another MMR gene or *MGMT* (Fig. 3a, b, Fig. S2). We also identified a clonal TMZ-associated mutation in *MGMT* of unknown significance in the recurrent tumor of patient 18. In the initial and recurrent tumors of the TMZ-non-HM ($n = 4$) patients, MMR pathway genes were intact, but heterozygous loss of *MGMT* was detected in the initial tumor of patient 11 and the recurrent tumor of patient 17. Interestingly, the recurrent tumor of patient 11 grew out from an earlier cell that retained both alleles of MGMT, while the recurrent tumor of patient 17 had decreased levels of DNA methylation at *MGMT* (initial 28.3 %, recurrence 12.7 %), indicating that in both cases MGMT levels may not have been impaired during TMZ treatment and recurrence. In the non-TMZ group ($n = 24$), mutational analysis was performed in patients of which sufficient DNA from matched normal and initial and recurrent tumor was available ($n = 7$). In these seven cases, only one MMR mutation was detected, an *MSH3* mutation in the initial tumor but not in the recurrent tumor of patient 07. DNA copy number status of *MGMT* and MMR genes was available for 21 of 24 patients in the non-TMZ subgroup. Genomic loss affecting the *MGMT* region was detected in five initial and seven recurrent tumors of the non-TMZ subgroup. Similarly, deletion encompassing an MMR gene was shared between the initial and recurrent tumors of five cases, while four patients acquired a deletion encompassing a MMR gene at recurrence (Supplementary Table S3). As these patients did not receive TMZ, it is not known how TMZ treatment may have affected *MGMT* methylation levels at recurrence, or if the identified genetic alterations to *MGMT* and MMR genes may indicate a susceptibility to hypermutation.

Discussion

We compared spontaneous and treatment-associated evolution of DNA repair deficiency in a cohort of 34 initial LGG and their patient-matched recurrences. Our data suggest MGMT and MMR-mediated DNA repair may be compromised by sequential and coincident loss of heterozygosity, methylation [44], and TMZ-associated mutation, although repair activity could not be tested directly. Considering prior studies of TMZ-treated GBM patients [1, 8, 26, 62] and cells treated with TMZ in vitro [5], our results suggest that TMZ-induced hypermutation is the consequence of a TMZ resistance mechanism in LGG. This putative mechanism is not fully understood, but may be induced directly

by the mutagenic action of TMZ on DNA repair genes, in combination with pre-existing and concurrent copy number alterations in cells with a higher level of *MGMT* methylation. The resistance mechanism appears to involve a switch from toxicity to tolerance of TMZ-induced DNA damage. The sequential acquisition of genetic and epigenetic change in MGMT and MMR genes in the TMZ-HM group differs notably from the patterns in patients who did not received TMZ, and in TMZ-treated but not hypermutated patients.

We observed a consistent increase over time in *MGMT* methylation level, which was not detected in LGG patients without a TMZ-associated hypermutator phenotype. The apparent positive selection of *MGMT* hypermethylated cells and a corresponding decrease in *MGMT* expression may predispose a cell to persistent O^6-methylguanine lesions and acquisition of MMR gene mutation, enabling hypermutation from subsequent rounds of TMZ treatment (Fig. 4). MGMT activity also may be decreased by TMZ treatment itself, as the MGMT protein is not regenerated following repair [52].

Other studies have addressed temporal changes of *MGMT* methylation in smaller cohorts of grade II astrocytomas [22, 30, 35] and GBMs [7, 9, 38] with MSP only, and without mutational and copy number analysis. In the present study, bisulfite sequencing of the *MGMT* promoter in 34 paired initial and recurrent tumors enabled detailed, quantitative analysis of temporal evolution in individual patients. Given the sample size, a meaningful comparison of *MGMT* methylation change was not possible for GBM recurrences that were HM ($n = 6$) versus GBM recurrences in the TMZ-non-HM subgroup ($n = 1$). We observed a distinct pattern of increased *MGMT* methylation level between initial and patient-matched, TMZ-treated and hypermutated recurrences.

Exposure of cells to a mutagen such as TMZ will result in a different set of mutations in each cell within the population. However, our detection of somatic mutations in MMR-related genes in hypermutated DNA derived from bulk samples strongly suggests that these recurrences are derived from clonal expansion from a very small number of hypermutated cells [26]. The mutations are predominantly C>T/G>A transitions, the type of mutation known to be induced by TMZ treatment. Literature on the functionality of these mutations varies, for example somatic mutations *MLH1* P648L and P640S in the TMZ-treated recurrent tumors of patients 1 and 10 also occur in the germline of families with hereditary nonpolyposis colon cancer, significantly affect MLH1 protein function, and are predicted to be pathogenic [10, 20, 43, 51]. The splice site mutation in MSH3 of patient 18 leads to a single-nucleotide shift of the splice acceptor site, resulting in an out-of-frame transcript and premature truncation of the protein. However, the role of MSH3 in cancer is less clearly defined [39]. In MMR-deficient cells, futile cycling of MMR repair does not occur, enabling this type of mutation. The C>T/G>A

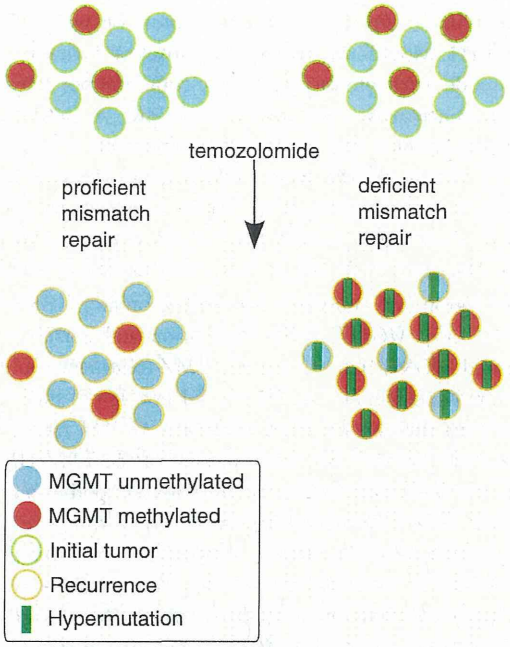

Fig. 4 A working model of the effect of an impaired MMR system on clonal outgrowth of *MGMT* methylated cells during acquisition of the TMZ-associated hypermutator phenotype and TMZ-associated malignant progression. *Left:* when MMR is intact, TMZ treatment induces cell death in *MGMT* methylated cells. The histology of the recurrent tumor is variable. *Right:* when MMR is deficient, TMZ treatment fails to induce cell death and *MGMT* methylated tumor cells may expand, become hypermutated, and undergo malignant progression to GBM

mutation also occurs spontaneously, however, the extreme number of new mutations, the strong bias towards C>T/G>A versus other mutations, and the occurrence of hypermutation after TMZ treatment but not in patient-matched pre-treatment samples suggests TMZ is the predominant source. The proportion of tumors developing a hypermutation profile after TMZ treatment in our series is 60 % (6 out of 10). This cohort and others [1, 26] are too small to determine the actual incidence of hypermutated diffuse gliomas after alkylating agent chemotherapy.

Biomarkers of susceptibility to TMZ-associated hypermutation could have significant clinical value. Rare germline and somatic *MSH6* mutations that might affect how cells respond to TMZ have been detected in patients with untreated anaplastic oligodendrogliomas and GBMs [36, 46]. Within our small cohort, we found that loss of heterozygosity spanning MMR genes was unique to the TMZ-HM group relative to TMZ-non-HM group. In three TMZ-HM patients, the initial tumor showed deletion of *MGMT* or an MMR gene. The copy number data of two of the other initial tumors from the TMZ-HM group were ambiguous. In a study of MMR protein expression assessed by